Development and Control of an Integrated and Distributed Inverter for a Fault Tolerant Five-Phase Switched Reluctance Traction Drive

Martin D. Hennen, *Student Member, IEEE*, Markus Niessen, Christian Heyers, Helge J. Brauer, *Student Member, IEEE*, and Rik W. De Doncker, *Fellow, IEEE*

***Abstract*—A concept of an integrated and distributed inverter for switched reluctance machines is introduced. The application at hand is an outer-rotor direct drive designed for railway traction applications. A five-phase switched reluctance machine was developed and is used to demonstrate the function of the integrated and distributed inverter. The distribution is achieved by supplying each phase coil with its own modular inverter. Each inverter module is placed evenly around the end of the stator stack next to its dedicated coil. This increases the redundancy of the drive significantly. The likelihood of phase-to-phase faults is reduced, because no overlapping end-turns are necessary. Also, the integration of machine and inverter is simplified, because the semiconductors can be evenly distributed around the machine. The concept reduces the amount of terminals between drive and vehicle to communication, power supply, and cooling, independent of the number of machine phases. With the integrated and distributed inverter new control strategies can be developed to influence machine vibration and radiated noise. In this paper, the design of the prototype, the direct torque control of the five-phase machine, and the behavior in the case of a fault inside a module is analyzed.**

***Index Terms*—Direct torque control, fault tolerance, inverter, outer-rotor switched reluctance machine.**

I. Introduction

CONSIDERING the specifications of a direct drive for railway traction, i.e., low speed and high torque, an outer-rotor switched reluctance machine has several advantages compared to an inner-rotor design. In particular, the efficiency of the outer-rotor machine is higher, due to its improved torque per ampere ratio, as shown in [1] and [2]. This is due to the fact, that the air gap radius of the outer-rotor machine can be made larger since the windings and the cooling are located in the center of the machine. The prototype machine, as introduced in [2] by the authors has a nominal torque of 1800 N·m at 350 r/min and maximum speed of 750 r/min. Fig. 1 shows the cross section of the machine with 20 stator and 16 rotor teeth. The machine was designed using the analytical tool PC-SRD from SPEED consortium at University of Glasgow [3]. Details on switched reluctance machines (SRMs) and how to design can be found, for example, in [4] and [5].

TABLE I
Specifications of the Designed SRM

Stator / rotor tooth configuration (N_s, N_r)	20/16
Phase number	5
Outer rotor radius	320 mm
Inner rotor radius	259 mm
Outer stator radius	257.5 mm
Inner stator radius	150 mm
Stack length	150 mm
Airgap	1.5 mm
Number of turns per coil	160
Nominal torque	1800 Nm
Nominal power	67 kW
Max. speed	750 rpm

The specifications of the prototype are given in Table I. It has to be noted that due to the geometry of the slot area of the outer-rotor design and the design of the concentrated coils, the copper fill factor of the prototype is 60%. This is high compared to rotating field machines which normally reach 30% to 40%. Furthermore, the air gap of 1.5 mm is similar to what is used in induction and synchronous machines in railway traction applications.

A drawback of SRMs is the need for two terminal connections per phase, which have to be routed to the inverter in the case of a classical drive concept. Most connectors and cable leadthroughs can be avoided by integrating the inverter, reducing the required terminals to provide dc-link power, communication, and cooling. This simplifies the integration of the machine in the boogie. The inverter is placed in the center of the machine, as shown in Fig. 2. A similar approach where the inverter is modularized and integrated with the machine is the *integrated modular motor drive* as shown in [6]. The concept is used for a modular permanent magnet machine. In this paper, a concept for an SRM where the inverter is divided into one module per stator coil is analyzed.

It is well known that SRMs have intrinsically a high redundancy, due to the fact that the SRM can continue operation in the case of a fault inside a phase, as shown, for example, in [7]–[11]. In contrast to rotating field machines, the phases are electrically and almost magnetically independent [9]. In [12] and [13], the

Manuscript received August 24, 2010; revised January 22, 2011; accepted March 7, 2011. Date of current version January 9, 2012. This work was supported by the German Research Foundation for the development of the drive under Project DO618/24-1. Recommended for publication by Associate Editor M. Degner.

The authors are with the Institute for Power Electronics and Electrical Drives, RWTH Aachen University, 52066 Aachen, Germany (e-mail: he@isea.rwth-aachen.de; markus.niessen@isea.rwth-aachen.de; Christian.Heyers@rwth-aachen.de; be@isea.rwth-aachen.de; dedoncker@ieee.org).

Color versions of one or more of the figures in this paper are available online at http://ieeexplore.ieee.org.

Digital Object Identifier 10.1109/TPEL.2011.2132763

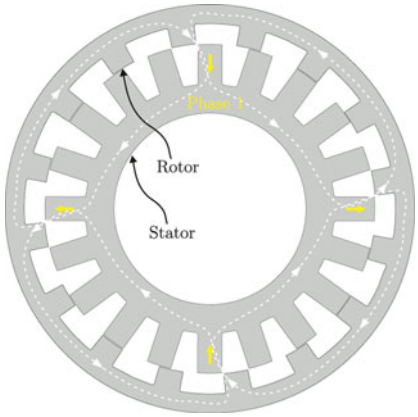

Fig. 1. Cross section of 16/20 SRM.

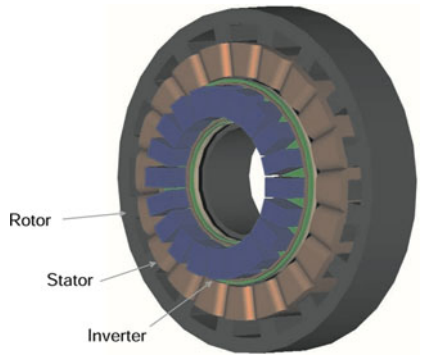

Fig. 2. Concept of the SRM with integrated and distributed inverter.

resulting speed, torque, and current ripple for open- and short-circuit faults are shown.

Using the distributed inverter, it can be seen that the pole modules within one phase are electrically independent. It will be investigated, how a fault inside a module influences the operation of the drive. A detailed analysis of the possible faults in the machine, the inverter, or a single pole module is necessary to understand the impact of these faults on the operation and performance of the integrated inverter SRM drive. To determine the influence of a fault, different characteristics, such as torque ripple, average torque, vibration, and noise are analyzed.

Section II details the concept of the inverter and the built prototype. In Section III, the communication concept between pole modules and a superior control is shown. Subsequently, the torque control (*predictive PWM-DITC*) for multiphase switched reluctance machines is illustrated in Section IV [14]. Sections V and VI will give results of simulation and measurements, respectively.

II. Design of Integrated and Distributed Inverter

Standard inverters for switched reluctance machines consist of one asymmetrical half-bridge per phase, having two switches and two diodes. The benefit of this inverter topology together with an SRM is the magnetic and electric decoupling of the machine phases. The machine is inherent redundant, meaning, with the lack of one or more phases, the remaining phases can continue operation.

TABLE II
Specifications of Pole Module

DC-link voltage	400 V
Capacitance (film capacitor)	33 μF
Nominal phase current (rms)	30 A
Nominal power	3.4 kW

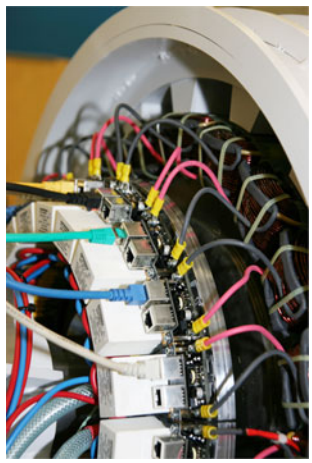

Fig. 3. Prototype of drive.

The key idea of the distributed inverter is to use an asymmetrical half-bridge inverter module to supply every coil of a phase individually. By developing the distributed inverter, the inherent redundancy of the SRM is hence increased further. In the case of a failure of a pole module, the remaining modules of the phase can continue operation. The prototype of the inverter was built with 20 separate pole modules, each supplying a single coil. Each pole module uses standard discrete semiconductors. Consequently, the integration of machine and inverter is simplified and the losses inside the semiconductors are distributed equally among all modules, which improves the cooling performance of the inverter greatly. A drawback is the higher amount of components, which leads to higher costs compared to a standard inverter. A way to reduce costs is the integration of each module itself to an integrated power module and a large-scale production of these modules.

Table II summarizes the electric specifications of the pole modules. Another advantage is the reduced complexity of the end-windings as can be seen in Fig. 3. The coils can be directly connected to the inverter. This also reduces the possibility of phase-to-phase faults.

From Fig. 3, it can be seen that each module has a film capacitor (white block). All capacitors of the modules are connected in parallel and together they build the dc-link capacitance of the inverter.

III. Communication Concept of Inverter

The challenge of the distributed inverter with 20 modules is to communicate with each module within one time step of the *pulsewidth modulation* (PWM). The proposed controller uses a PWM with a frequency of 10 kHz. Therefore, the control needs to read the measured currents, calculate the reference duty cycle

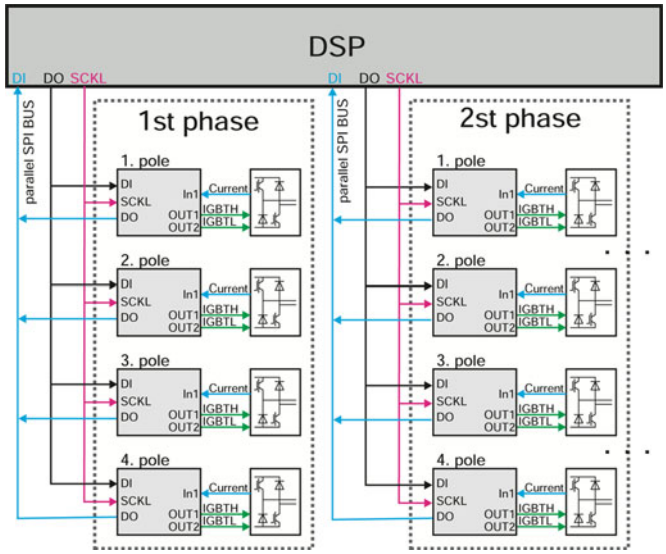

Fig. 4. Communication structure of prototype.

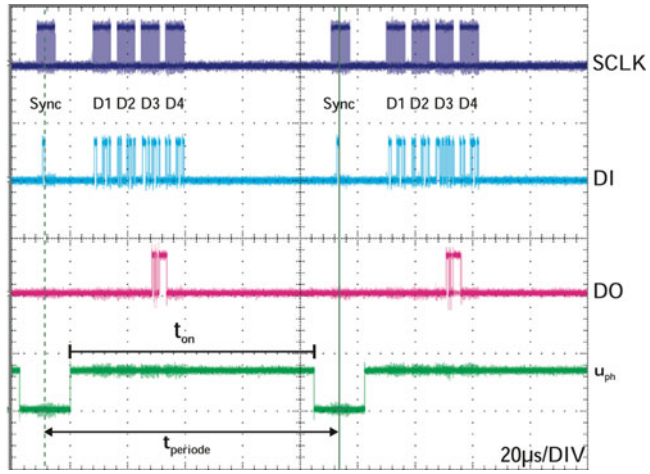

Fig. 5. Measured communication (SCKL, DI, DO, and u_{ph}).

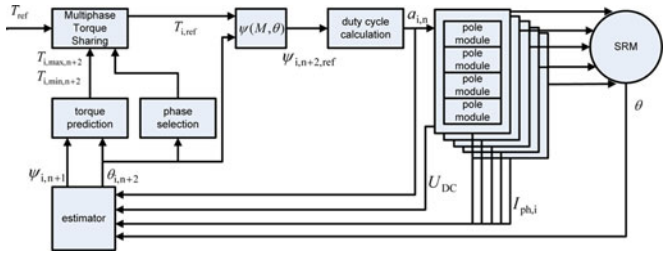

Fig. 6. Predictive PWM-DITC for distributed inverter.

and send it to the modules within 100 μs. To reduce communication time, a parallel, bidirectional protocol was developed. Parallel, because the digital signal processor (DSP) communicates with each of the five phases at the same time. The four modules of a phase are read serial. Bidirectional, because the reference duty cycle is transmitted and the measured current is received simultaneously. Fig. 4 shows the realized communication structure of the inverter. Two signals, *data in* (DI) and *data out* (DO), are used to transfer the data. The clock SCKL (standard clock) is used to synchronize the data of DI and DO.

The developed communication protocol contains the data, an access control, a command structure, and a fault detection system to detect single bit faults. Each pole module has a defined address inside his phase (1–4). With this address, the DSP can directly communicate with the module. The data are sent to the module with a 16-bit word that contains the address (3 bits), the command (3 bits), the reference duty cycle (8 bits), and the parity (2 bits). The measured current is sent back parallel to the duty cycle with 8 bits and a parity bit. Additionally, a 16-bit data word is sent once a phase is turned ON to synchronize the modules. All in all, for four modules, 4*16 bits(address, command, duty cycle, parity) + 16 bits(sync) + 4* 9 bits(current) = 116 bits are transmitted in one period per phase.

Assuming an allowed transmit time of 1/3 of a PWM period, the data rate is 3.48 Mbits/s. Because duty cycle and measured current are transmitted simultaneously, the necessary communication frequency reduces to 2.5 MHz. The remaining 2/3 of the 100 μs PWM period are available for the calculation of the duty cycle.

The communication, as well as the generation of the switching signals, overcurrent protection, etc., is realized on a *complex programmable logic device* (CPLD) on each pole module. The module receives the aforementioned address, command and duty cycle, sets the switching signals and sends back the measured current. Additionally, once in an electrical period, after the module has been turned OFF, a temperature measured on the PCB of each pole module is sent back. Fig. 5 shows an example of a measured communication with one phase. The figure shows the signals SCKL, DI, and DO, as well as the measured phase voltage u_{ph} of one module. The communication starts by sending the SYNC command to all modules, which triggers the PWM period. After that the communication continuous by talking to the four modules of the phase in series. Each module receives a data word (D1–D4). In the figure, only the third module is asked to send back its measured current (DO signal). It can be seen that during the communication, the modules apply the duty cycle that was received in the previous period.

IV. Implemented Torque Control

To control the torque of the five-phase machine, a torque control strategy, introduced in [15], is used. The *predictive PWM-based direct instantaneous torque control* (PWM-DITC) was enhanced to be able to work with more than three active phases simultaneously. To do this, the *multiphase torque sharing algorithm* was developed [14].

A block diagram of the implemented control is shown in Fig. 6. The interface between control and inverter is the reference duty cycle for phase $a_{i,n}$, where *i* is the phase number and *n* the index of the actual sample time t_n. As input, the control needs the reference torque T_{ref}, the measured current $i_{i,n}$, the dc-link voltage u_{dc}, and the actual rotor position θ.

In *predictive PWM-DITC* the phase current at sample time t_n is measured and the flux linkage in the next sample time t_{n+1} is predicted based on the previous calculated duty cycle. In the next step, the controller estimates the flux linkage and rotor position

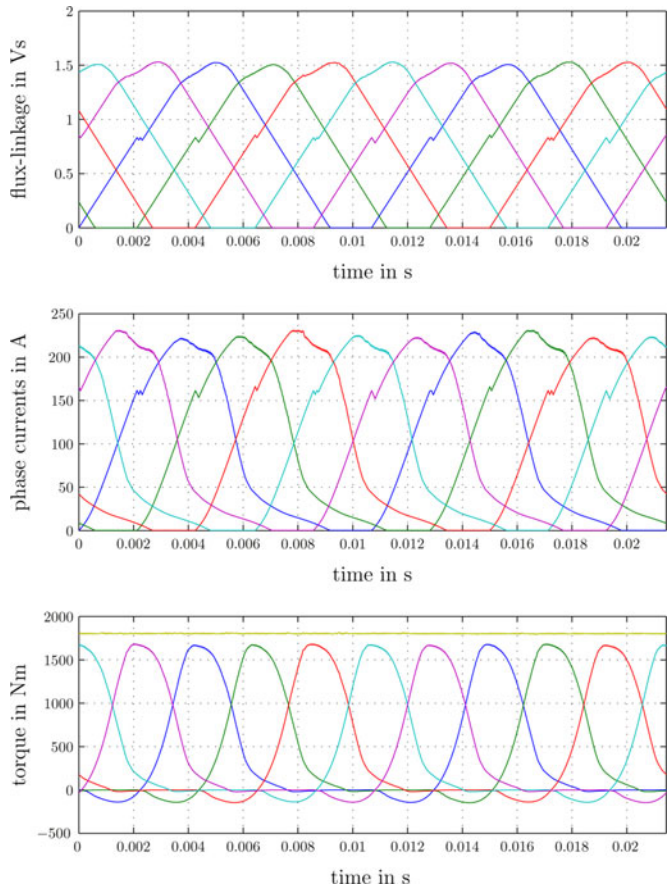

Fig. 7. Simulation results at 1800 N·m at 350 r/min (1.59% torque ripple).

for the next sample time t_{n+2} to determine the maximum and minimum torque for maximum and minimum duty cycle of $a_{i,n+1,\max} = 1$ and $a_{i,n+1,\min} = -1$. The multiphase torque sharing algorithm shares the reference torque between the active phases, and determines the reference torque per phase $t_{i,\mathrm{ref}}$. From the reference torque per phase, the duty cycle per phase is calculated. In contrast to the control developed in [14], the calculated duty cycle is now transmitted to the 20 pole modules. The measured phase current used for the control is built of the average of the four pole module currents of a phase.

The control was implemented and tested in a MATLAB/Simulink model. The machine is modeled using a $\Psi(I,\theta)$ and a $T(I,\theta)$ characteristic, which is flux linkage Ψ and torque T depending on phase current I and rotor position θ. These characteristics can either be simulated with finite elements, or measured on a test bench, as shown in [16]. A detailed description of the model can be found for example in [17].

Fig. 7 shows the simulation results for reference torque and speed of 1800 N·m at 350 r/min. Shown is the flux linkage per phase, the phase currents, the torque per phase, and the total torque. In this operating point, the total average torque is 1803 N·m with a maximum ripple of 1.52%.

The torque ripple was simulated for the complete operating range of the machine. The reference torque was varied between $0 \leq T_{\mathrm{ref}} \leq 1800$ N·m. The reference speed between $0 \leq n_{\mathrm{ref}} \leq 750$ r/min. For each operating point, the average torque and

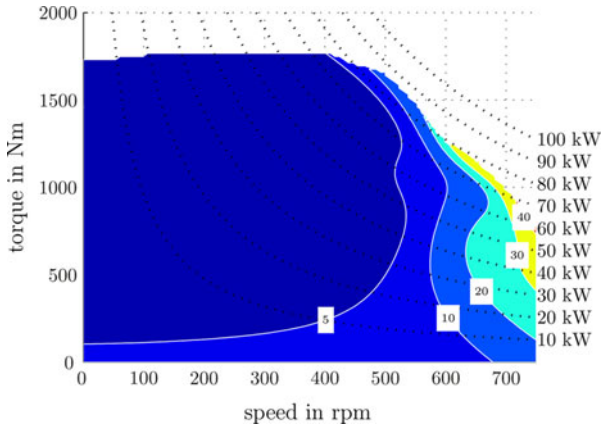

Fig. 8. Simulated torque ripple over operating range in percent of reference torque.

the torque ripple was calculated. The resulting torque and the reference speed was used to plot a diagram of torque ripple over average torque and speed, as shown in Fig. 8. It can be seen, that over a wide operating area, the torque ripple is beneath 10%. At higher speeds the torque ripple increases. This is due to single pulse operation of the machine. At maximum speed and torque, the torque ripple reaches up to 40%.

V. Fault Tolerance Analysis

In [9], it was shown that whether the coil of a disconnected phase is open- or short-circuited makes little difference to the performance of the machine. Due to the negligible mutual coupling of the phases, the induced current in a shorted phase remains low. If the distributed inverter is considered, the mutual coupling of the phases remains low, but the coupling of the poles of one phase has to be considered.

In the following, it is investigated how an open-circuit fault inside a module or a single coil influences the operation of the drive. To determine the influence of a fault, different parameters, such as average torque, torque ripple, vibration, and noise are analyzed. It is apparent, that an asymmetric excitation of the four poles of a phase leads to a force on the rotor, stressing the bearings. The net radial force on the rotor is called the *unbalanced magnetic pull*, as described in [18]. To simulate short-circuit faults, a transient simulation of the machine is necessary, because the short-circuit current depends on the rate of change of the flux linkage in the coil. Developing a model including short circuit faults is part of future work.

A. Average Torque and Torque Ripple

The developed MATLAB/Simulink model of the five-phase machine is used to show the influence of faults in pole modules on the average torque and the torque ripple. Fig. 9 shows the results of the simulation for a control without any fault compensation or feedback to the control. Fig. 9(a)–(e) shows the results for no fault up to four faulty modules of the same phase. From the results, the inherent fault tolerance of the switched reluctance machine can be seen. If one out of twenty modules fails, the torque is reduced by approximately 90 N·m, which

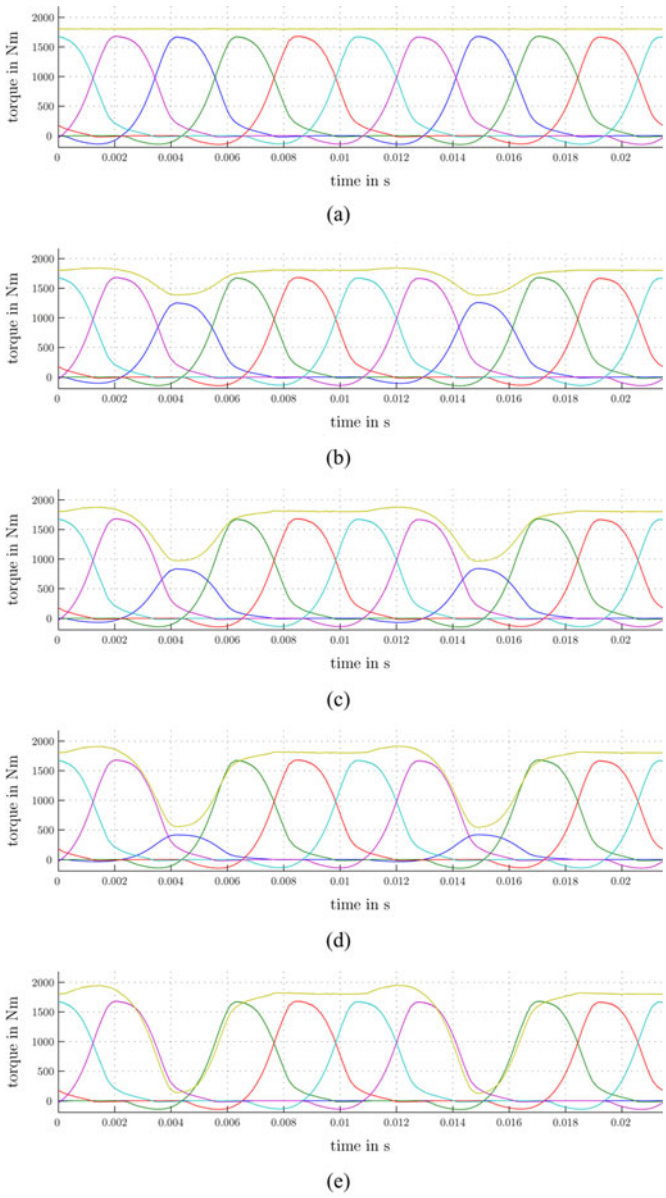

Fig. 9. Simulated torque for faults in pole modules. (a) $4/4$ modules, 1.52% torque ripple, 1803 N·m average torque. (b) $3/4$ module, 25.4% torque ripple, 1714 N·m average torque. (c) $2/4$ module, 49.1% torque ripple, 1625 N·m average torque. (d) $1/4$ module, 71.9% torque ripple, 1536 N·m average torque. (e) $0/4$ module, 93.9% torque ripple, 1447 N·m average torque.

is approximately $1/20$ of the reference torque. After all four modules of a phase have failed, the torque is reduced $1/N_{\mathrm{ph}}$, hence, 20% of the reference torque. The torque ripple in case no fault compensation is applied, increases with each failing module approximately by 25%. If the complete phase fails, the torque ripple is nearly 100% at the simulated operating point.

These results show the influence of faults on the average torque and the torque ripple. What is more important is the spatial orientation of the forces on the rotor. The orientation of the force for each rotor tooth has to be known to first calculate the unbalanced magnetic pull on the bearings as sum of all tooth forces, and second, to get an idea about the different resulting vibration modes of the rotor.

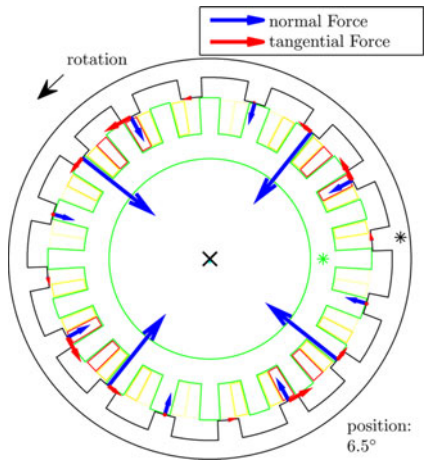

Fig. 10. Normal and tangential forces on rotor for no fault.

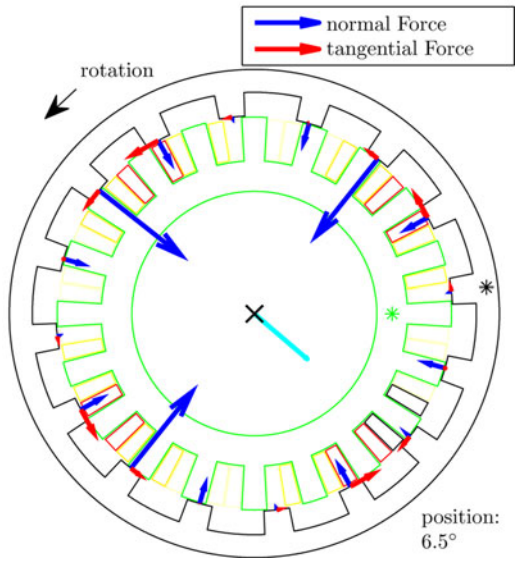

Fig. 11. Normal and tangential forces on rotor for one fault.

B. Unbalanced Magnetic Pull

To calculate the radial and tangential forces on each rotor tooth, the 2D FEM simulation used to calculate the machines characteristics in Section IV is used. Additional to flux and torque, the normal and tangential forces on the teeth, depending on current and rotor position are exported as a characteristic. Due to the magnetic coupling of the modules within one phase, each failure type (one, two, three... failing modules) has to be simulated in FEM and exported separately as a characteristic. These characteristics can be included in the simulation model as lookup tables to get the forces on the rotor teeth, depending on the number of active pole modules per phase. Fig. 10 shows the normal and tangential forces for 1000 N·m and 350 r/min at an arbitrary rotor position for no faults. To see the influence of open circuit failing modules, the corresponding modules can be turned OFF separately. As an example, the resulting forces for one failing module at the same operating point and position as Fig. 10 are shown in Fig. 11. As expected, the loss of one module results in an unbalanced magnetic pull, shown as vector

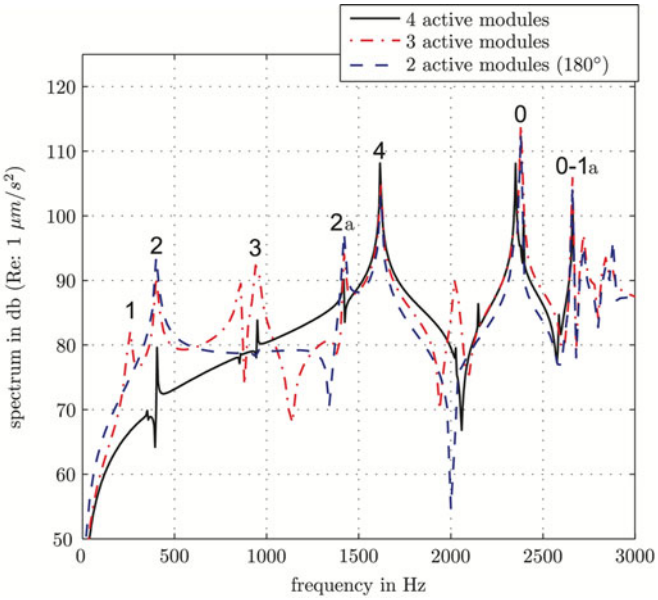

Fig. 12. Simulated spectrum of displacement.

in the center of the machine. The amplitude depends on the operating torque, and reaches up to 8500 N at nominal torque of 1800 N·m. This force is excited periodically every electrical period; hence, the frequency of the magnetic pull is the multiplication of speed and number of rotor teeth ($n \cdot N_r$). In this example, at 350 r/min and 1000 N·m, the unbalanced pull has a frequency of approximately 100 Hz and an amplitude of 4600 N.

C. Vibration Shapes

After the analysis of average torque, torque ripple, and unbalanced magnetic pull, it is analyzed how a fault inside a module influences the resulting vibration shapes of the machine. The shapes depend on the normal and tangential forces applied to the rotor, as shown in Figs. 10 and 11. To analyze the possible vibration shapes of the machine, a structural dynamic simulation of the outer rotor, including the housing is performed. With a modal analysis the eigenfrequencies of the machine can be simulated. Each eigenfrequency corresponds to certain vibration shape or mode. To find out which modes are excited during operation of the machine, a harmonic analysis with constant force excitation and varying frequency is done. The forces are applied to the four poles of one phase. This simulation returns a transfer function of force to surface acceleration of the machine. The peaks of this function show the excited modes. To simulate the real behavior of the prototype at the test bench, the rotation, the excitation of several phases simultaneously, and the frequency composition of the forces has to be taken into account, as shown in [19]. This is not in the scope of this paper, hence, the simulation results of the surface acceleration can only be used as a basis to determine the vibration shapes of the prototype machine at the test bench for different faults, as done in Section VI.

Fig. 12 shows the simulation results for four, three, and two opposite excited pole modules. In the case of no fault, the main frequency components are at 1600, 2350, and 2700 Hz. The modal analysis shows that at these frequencies the mode 4, mode 0, and mode 0 with a superimposed mode 1 in axial direction is excited (mode 0–1a). The modes in axial direction are due to the one-sided mounting of the prototype. The numbers in Fig. 12 represent the modes corresponding to the frequencies, which where found with the modal analysis. In Fig. 13, the shapes of the modes for the frequency peaks in Fig. 12 are shown. As expected for a four-pole machine, the main vibration modes are 4 and 0.

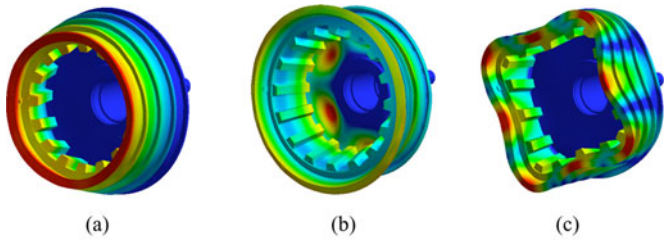

Fig. 13. Excited vibration shapes for no fault from modal analysis. (a) Mode 0. (b) Mode 0–1a. (c) Mode 4.

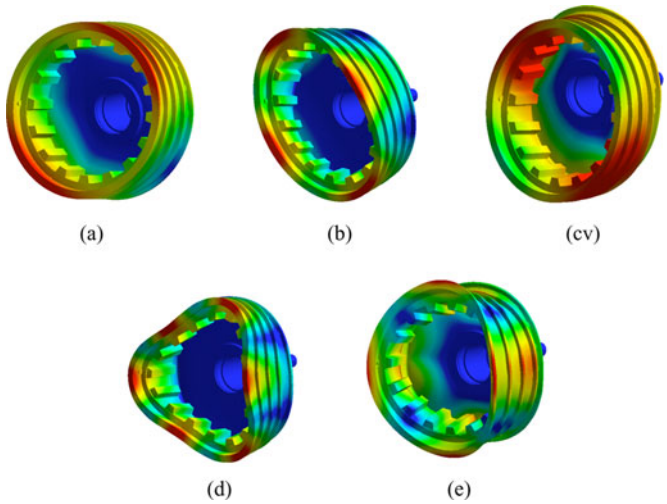

Fig. 14. Additional excited vibration shapes for one fault from modal analysis. (a) Mode 1. (b) Mode 2. (c) Mode 1–1a. (d) Mode 3. (e) Mode 2 axial.

To simulate a fault with the structural dynamic simulation, the force of one pole was set to zero, respectively, for other number of faults. As shown in Fig. 12, a fault of one module results in several additional frequency components. The additional modes are mode 1 (250 Hz), mode 2 (400 Hz), mode 3 (950 Hz), and a mode 2 in axial direction (mode 2a, 1400 Hz). The shapes of the additional resulting modes due to the fault are shown in Fig. 14.

Due to the asymmetric excitation, the vibration increases significantly and the magnetic pull on the rotor stresses the bearings. Without any fault compensation from the remaining modules, which is part of the future work on this prototype, the simplest way to reduce the vibration is turn OFF the module opposite the faulty module and restore a symmetric excitation with zero magnetic pull. The results of the simulation for two active opposite modules are also shown in Fig. 12. It can be seen, that modes 1 and 3 are not excited. This reduces the level of vibration significantly. The modes 2 and 2a remain, as is clear due to the two pole symmetric excitation.

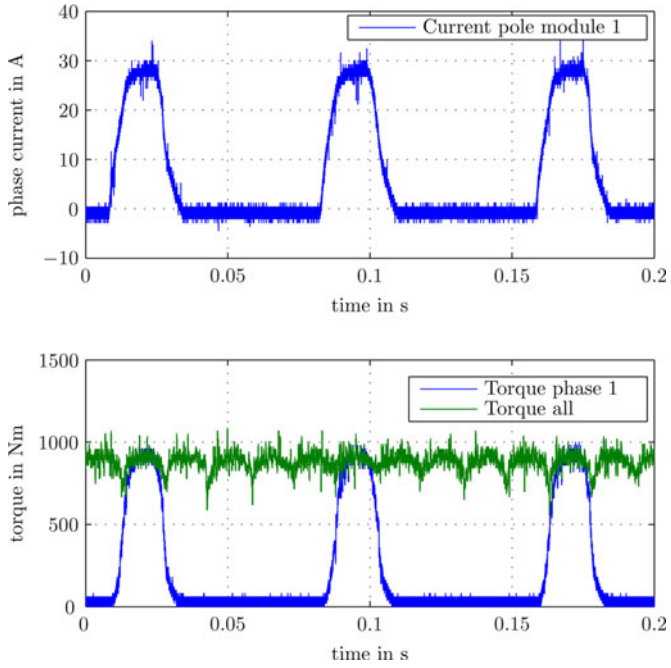

Fig. 15. Measurement results at 900 N·m and 50 r/min.

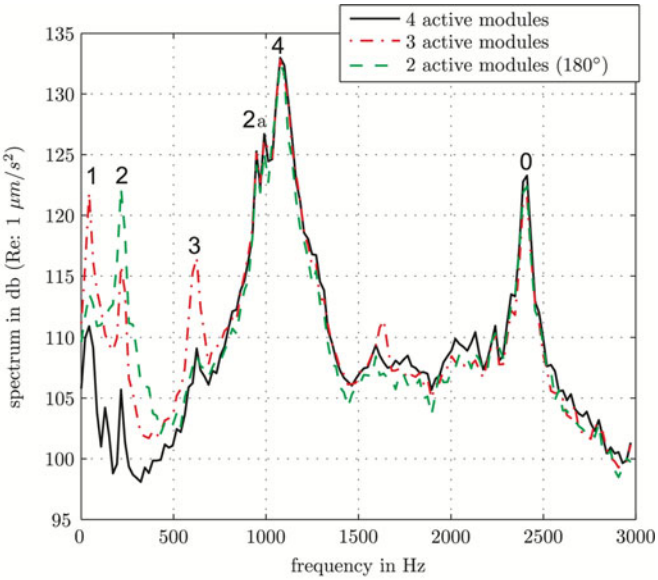

Fig. 16. Measured spectrum with vibration sensor on the rotor at 350 N·m and 50 r/min.

VI. Measurement Results

To test the communication and the implemented control, the drive was operated on the test bench. Fig. 15 shows the measured results at an operating point of 900 N·m and 50 r/min. The figure shows the measured current of one pole module, the torque of the corresponding phase, and the overall torque determined by the control. The torque was recorded using analog outputs of the DSP. The current has a peak value of 30 A (16 A_{rms}). The measured torque with a torque transducer at the shaft was 806 N·m.

In comparison to the simulation, the overall torque has a ripple of approximately 25%. This is caused by the use of the simulated characteristics. To reduce the ripple, the simulated characteristics and the calculated *turn-on* and *turn-off* angles of each phase have to be fitted to the built prototype. Note that the phases turn ON too late. Hence, the total torque during the commutation of one phase to the next is not correctly controlled. However, the results show the basic functionality of the developed drive.

To verify the simulated vibrations during operation with and without faults, the acceleration on the rotor surface was measured using vibration sensors. The signal of the sensors were transmitted to a pc using a telemetry unit fixed on the rotor. Due to the previous shown unbalanced magnetic pull in the case of an asymmetric excitation, an operating point of 350 N·m and 50 r/min was chosen. At this point, the resulting unbalanced forces on the rotor are tolerable. The vibration was measured for no, one, and two opposite faults, analog to Section V-C. Fig. 16 shows the measured spectrum of the surface acceleration.

The main difference between measurement and simulation is the absolute frequencies of the modes (except mode 0). For example, in the measurements mode 4 is at approximately 1100 Hz, instead of 1600 Hz for the simulation. To improve the results, the stiffness of the simulation model can be fitted to the actual built prototype, including construction tolerances and different material parameters. Nevertheless, the simulation results can be used to identify excited modes during operation of the prototype.

The increase of vibration at low frequencies in the case of a single module fault is shown clearly in the figure. Especially, the asymmetric mode 1 in Fig. 16 at 43 Hz stresses the single side mounted rotor, leading to a severe additional mechanical noise. In the third case, where the opposite module is turned OFF, only an additional resonance at 250 Hz remains. This corresponds to the mode 2, as was simulated (see Fig. 12). Restoring a symmetric excitation and hence, the prevention of mode 1 and 3 reduce the mechanical noise of the machine significantly. Compared to no fault, the level of noise is still increased. In future work, it is analyzed how a control of the normal forces of each module can decrease vibrations in the case of different faults.

VII. Conclusion

The concept of an integrated and distributed inverter for an outer-rotor switched reluctance machine was introduced. The integrated inverter allows to increase the number of machine phases without increasing the number terminals. This simplifies the integration of the drive in the application. The high number of phases increases the redundancy of the drive. The phases are magnetically and electrically decoupled. Additionally, due to the modular design, each pole of a phase is electrically decoupled. A direct torque control for the developed drive was implemented and tested. It was found that the simulated 2-D FEM machine characteristics, used by the control, need to be adapted to the built prototype to optimize the control of the torque. The simulation has shown that over a wide operating area, the torque ripple is below 10%.

Simulation and tests show that the drive can continue operation in the case of open-circuit faults of single pole modules. The effect on torque ripple and vibration was simulated and verified on the test bench. In the case of a fault of a single module, additional vibration modes and a magnetic pull on the rotor occur, caused by the asymmetric excitation. This increases the radiated noise significantly, but can be reduced by turning OFF the opposite module, restoring a symmetric excitation. Then, only an additional mode 2 is excited. The built model and the prototype of the drive allow to further analyze fault tolerant control strategies to actively reduce the emerging vibrations and enhance the operating area in the case of different faults. Also, the analysis of short-circuit faults in the inverter and the machine are part of future work.

REFERENCES

[1] R. B. Inderka and R. W. De Doncker, "Outside-rotor switched reluctance machine for minimal hybrid vehicle application," presented at the 17th Int. Electr.-Veh. Symp., Montreal, Canada, 2000.

[2] M. D. Hennen and R. W. De Doncker, "Comparison of outer- and inner-rotor switched reluctance machines," in *Proc. 7th Int. Conf. Power Electron. Drive Syst.*, 2007, pp. 702–706.

[3] T. J. E. Miller, *PC-SRD* SPEED Consortium, Dept. of Electron. and Electr. Eng., Univ. of Glasgow, Glasgow, U.K., 2008.

[4] T. J. E. Miller, *Switched Reluctane Motors and their Control*. London, U.K.: Oxford Univ. Press, 1993, ISBN 0 19 859387 2.

[5] T. J. E. Miller, "Optimal design of switched reluctance motors," *IEEE Trans. Ind. Electron.*, vol. 49, no. 1, pp. 15–27, Feb. 2002.

[6] N. Brown, T. Jahns, and R. Lorenz, "Power converter design for an integrated modular motor drive," in *Proc. 42nd IAS Annu. Meeting. Conf. Rec. 2007 IEEE*, pp. 1322–1328.

[7] A. A. Arkadan and B. W. Kielgas, "Switched reluctance motor drive systems dynamic performance prediction under internal and external fault conditions," *IEEE Trans. Energy Convers.*, vol. 9, no. 1, pp. 45–52, Mar. 1994.

[8] V. K. Sharma, S. S. Murthy, and B. Singh, "Analysis of switched reluctance motor drive under fault conditions," in *Proc. IEEE 33rd IAS Annu. Meeting, 1998*, vol. 1, pp. 553–562.

[9] C. M. Stephens, "Fault detection and management system for fault-tolerant switched reluctance motor drives," *IEEE Trans. Ind. Appl.*, vol. 27, no. 6, pp. 1098–1102, Nov. 1991.

[10] T. J. E. Miller, "Faults and unbalance forces in the switched reluctance machine," *IEEE Trans. Ind. Appl.*, vol. 31, no. 2, pp. 319–328, Mar./Apr. 1995.

[11] A. Arkadan and B. Kielgas, "The coupled problem in switched reluctance motor drive systems during fault conditions," *IEEE Trans. Magn.*, vol. 30, no. 5, pp. 3256–3259, Sep. 1994.

[12] I. Husain and M. N. Anwar, "Fault analysis of switched reluctance motor drives," in *Proc. Int. Conf. Electr. Mach. Drives*, 1999, pp. 41–43.

[13] S. Gopalakrishnan, A. M. Omekanda, and B. Lequesne, "Classification and remediation of electrical faults in the switched reluctance drive," *IEEE Trans. Ind. Appl.*, vol. 42, no. 2, pp. 479–486, Mar. 2006.

[14] H. J. Brauer, M. D. Hennen, and R. W. De Doncker, "Multiphase torque-sharing concepts of predictive pwm-ditc for srm," in *Proc. 7th Int. Conf. Power Electron. Drive Syst.*, 2007, pp. 511–516.

[15] C. R. Neuhaus, N. H. Fuengwarodsakul, and R. W. De Doncker, "Predictive PWM-based direct instantaneous torque control of switched reluctance drives," in *Proc. IEEE 37th Power Electron. Spec. Conf., 2006*, pp. 1–7.

[16] N. Fuengwarodsakul, S. Bauer, O. Tsafak, and R. De Doncker, "Characteristic measurement system for automotive class switched reluctance machines," in *Proc. Eur. Conf. Power Electron. Appl.*, 2005, p. 10.

[17] N. Fuengwarodsakul, R. De Doncker, and R. Inderka, "Simulation model of a switched reluctance drive in 42 v application," in *Proc. IEEE 29th Annu. Conf. Ind. Electron. Soc.*,, 2003, vol. 3, pp. 2871–2876.

[18] L. S. Stringer, "Unbalanced magnetic pull and shaft voltage in electromagnetic rotating machines," *Engineer*, vol. 225, no. 5856, Apr. 1968.

[19] M. Boesing, T. Schoenen, K. Kasper, and R. De Doncker, "Vibration synthesis for electrical machines based on force response superposition," *IEEE Trans. Magn.*, vol. 46, no. 8, pp. 2986–2989, Aug. 2010.

Martin D. Hennen (S'05) was born in Saarburg, Germany, in 1980. He received the Diploma degree in electrical engineering from the RWTH Aachen University, Aachen, Germany, in 2005.

Since November 2005, he has been a Research Associate at the Institute for Power Electronics and Electrical Drives, RWTH Aachen University, Aachen. His main interests include switched reluctance drives and their controls.

Markus Niessen was born in Offenbach, Germany, in 1981. He received the Diploma degree in electrical engineering from RWTH Aachen University, Aachen, Germany, in 2011.

Since 2010, he has been a Student Research Assistant at the Institute for Power Electronics and Electrical Drives, RWTH Aachen University, Aachen. His research interests include electrical traction drives for road-rail vehicles and power supplies.

Christian Heyers was born in Moenchengladbach, Germany, in 1981. He received the Diploma degree in electrical engineering from the RWTH Aachen University, Aachen, Germany, in 2007.

Since February 2008, he has been a Research Associate at the Laboratory for Machine Tools and Production Engineering, RWTH Aachen University, Aachen. He is currently involved in the realization of energy-efficient production systems.

Helge J. Brauer (S'09) received the Diploma degree in electrical engineering from the RWTH Aachen University, Aachen, Germany, in 2007.

Since 2007, he has been with the Institute for Power Electronics and Electrical Drives, RWTH Aachen University, where he is a Research Associate. His current research interests include high-temperature power electronics and the control of high-speed switched reluctance drives.

Rik W. De Doncker (F'01) received the Ph.D. degree in electrical engineering from the Katholieke Universiteit Leuven, Leuven, Belgium, in 1986.

In 1987, he was appointed as a Visiting Associate Professor at the University of Wisconsin, Madison. After a short stay as an Adjunct Researcher at IMEC, Leuven, he joined the General Electric Company at the Corporate Research and Development Center, Schenectady, NY, in 1989. In 1994, he joined Silicon Power Corporation (formerly GE-SPCO) as a Vice President of Technology. In 2006, he became the Director of the E.ON Energy Research Center at RWTH Aachen University, Aachen. During 2005–2006, he was a President of the IEEE Power Electronics Society (PELS). Since 2007, he has been a Board Member of the Energietechnischen Gesellschaft of the VDE in Germany. He was the Founding Chairman of the German IEEE IAS-PELS Joint Chapter. He is currently a Professor at RWTH Aachen University, Aachen, Germany, where he leads the Institute for Power Electronics and Electrical Drives.

Dr. De Doncker was a recipient of the IAS Outstanding Achievement Award in 2002.